Received 3 February 2019; revised 8 March 2019; accepted 21 March 2019. Date of publication 29 March 2019; date of current version 19 April 2019.
The review of this paper was arranged by Editor S. Reggiani.

Digital Object Identifier 10.1109/JEDS.2019.2907306

Operation Up to 500 °C of $Al_{0.85}Ga_{0.15}N/Al_{0.7}Ga_{0.3}N$ High Electron Mobility Transistors

PATRICK H. CAREY, IV [1], FAN REN [1] (Fellow, IEEE), ALBERT G. BACA [2], BRIANNA A. KLEIN [2], ANDREW A. ALLERMAN [2], ANDREW M. ARMSTRONG [2], ERICA A. DOUGLAS [2], ROBERT J. KAPLAR [2] (Senior Member, IEEE), PAUL G. KOTULA [2], AND STEPHEN J. PEARTON [3]

1 Department of Chemical Engineering, University of Florida, Gainesville, FL 32608, USA
2 Sandia National Laboratories, Albuquerque, NM 87815, USA
3 Department of Material Science and Engineering, University of Florida, Gainesville, FL 32608, USA

CORRESPONDING AUTHOR: P. H. CAREY, IV (e-mail: careyph@ufl.edu)

This work was supported by the Laboratory Directed Research and Development Program at Sandia National Laboratories, a multi-program laboratory managed and operated by National Technology and Engineering Solutions of Sandia, LLC, a wholly owned subsidiary of Honeywell Corporation, for the U.S. Department of Energy's National Nuclear Security Administration under Contract DE-NA0003525. The work of P. H. Carey, IV, F. Ren, and S. J. Pearton was supported in part by the Department of the Defense, Defense Threat Reduction Agency monitored by Jacob Calkins under Grant HDTRA1-17-1-011.

ABSTRACT AlGaN channel high electron mobility transistors (HEMTs) are the potential next step after GaN channel HEMTs, as the high aluminum content channel leads to an ultra-wide bandgap, higher breakdown field, and improved high temperature operation. $Al_{0.85}Ga_{0.15}N/Al_{0.7}Ga_{0.3}N$ (85/70) HEMTs were operated up to 500 °C in ambient causing only 58% reduction of dc current relative to 25 °C measurement. The low gate leakage current contributed to high gate voltage operation up to +10 V under $V_{ds} = 10$ V, with I_{ON}/I_{OFF} ratios of $> 2 \times 10^{11}$ and 3×10^6 at 25 and 500 °C, respectively. Gate-lag measurements at 100 kHz and 10% duty cycle were ideal and only slight loss of pulsed current at high gate voltages was observed. Low interfacial defects give rise to high quality pulsed characteristics and a low subthreshold swing value of 80 mV/dec at room temperature. Herein is an analysis of AlGaN-channel HEMTs and their potential future for high power and high temperature applications.

INDEX TERMS AlGaN, GaN, high electron mobility transistor (HEMT), high temperature.

I. INTRODUCTION

The established wide bandgap semiconductors GaN and SiC have superior material properties over Si and GaAs for use in high power and high frequency applications. GaN and SiC devices are being used in power conditioning systems, including pulsed power for avionics and electric ships, solid-state drivers for heavy electric motors, and advanced power management and control electronics. These power devices offer potential savings in both energy and cost because of their higher efficiency and power densities. Further improvements to high power switching devices include enhancing the breakdown field and the environmental operation regime [1]–[4]. To satisfy this demand, shifting from traditional GaN channel high electron mobility transistors (HEMTs) to AlGaN channel HEMTs is an attractive option for improving the power handling of the devices under extreme operation [1]–[13]. These new AlGaN channel devices are classified under the title of "ultra" wide bandgap materials (UWBG). The term can encompass any material with a bandgap larger than GaN (3.4 eV) such as AlN (6.2 eV) or Ga_2O_3 (4.9 eV).

One of the challenges of implementing these new AlGaN channel HEMTs is realizing low contact resistance. The two primary approaches have been through Si implantation [14] and selective growth of graded AlGaN [12], [15]–[18]. For the latter, low-damage etch processes are also needed [19]. The disadvantage of any impurity-doped HEMT is the effect of impurity scattering in high frequency operation, lowering the channel mobility and sheet carrier density [20]–[22]. High-quality selective regrowth for Ohmic contacts is not

FIGURE 1. Circular FET test structure of 85/70 HEMT.

yet a widely used method as it presents further manufacturing difficulties but provides a method for low resistance contacts for high-frequency operation.

$Al_{0.85}Ga_{0.15}N/Al_{0.7}Ga_{0.3}N$ HEMTs and other high aluminum content HEMTs have strong potential for future power and switching applications. One of the key reasons to pursue the high aluminum content is that the barrier layer becomes more insulator-like as the bandgap increases, further improving high junction temperature operation. Previous works have demonstrated excellent performance in both GaN and AlGaN channel devices with UWBG barrier layers at elevated temperatures [3], [4], [8], [23]–[25]. Additionally, use of the $Al_{0.85}Ga_{0.15}N/Al_{0.7}Ga_{0.3}N$ heterostructure benefits from a high-quality interface, due to almost perfect lattice matching as there is only a mild difference in aluminum content between barrier and channel layers [26]. Additionally, lower threading dislocation density is achieved through growth on AlN substrates as opposed to bare sapphire [27]. AlN has some advantages relative to GaN, as shown in Table 1, including a high breakdown electric field (12 MV/cm) and a high thermal conductivity (2.9 W/cm·K). While the calculated thermal conductivity of AlGaN is low, by using AlN as the growth substrate, device self-heating can be reduced. From a simple consideration of the physical properties, AlN-based devices may appear to be superior; however, they have particular difficulty with the formation of low resistance Ohmic contacts, thus the use of AlGaN alloys is beneficial [6], [28], in particular, AlGaN-channel HEMTs grown on AlN benefit from low leakage current, high ON/OFF ratio, and low subthreshold swing due to the commensurate growth structure [6]–[9].

In this work, DC and pulsed characteristics of $Al_{0.85}Ga_{0.15}N/Al_{0.7}Ga_{0.3}N$ HEMTs were explored from 25-500°C in ambient. The devices were characterized by analyzing their mobility, subthreshold slope, peak saturation current, and other relevant device parameters. These results further extend previous results on device operation to 200°C and demonstrate the excellent performance of $Al_{0.85}Ga_{0.15}N/Al_{0.7}Ga_{0.3}N$ HEMTs in the extreme temperature regime [9].

II. DEVICE FABRICATION AND TESTING

The HEMT samples were prepared by metal organic chemical vapor deposition (MOCVD) on sapphire substrates. First, a 1.6 μm thick AlN nucleation and buffer layer were grown on the substrate. Then a 50 nm transition layer from 100% aluminum to 70% aluminum was grown. Next, the 400 nm $Al_{0.7}Ga_{0.3}N$ unintentionally-doped channel layer was grown, capped by the 25 nm $Al_{0.85}Ga_{0.15}N$ barrier layer. The barrier layer was doped with Si at 3×10^{18} cm^{-3} for forming Ohmic contacts. Contactless measurement of the 2DEG sheet resistance yielded 2200 Ω/□, which combined with CV measurement gives a carrier density, n_s, of 9×10^{12} cm^{-2}. Circular HEMTs were fabricated with a gate length of 2 μm, and symmetric source/drain to gate spacing of 4 μm. The gate circumference was 660 μm. Planar Ti/Al/Ni/Au Ohmic contacts were deposited and subsequently annealed ($\rho_c = 2 \times 10^{-2}\Omega$-$cm^2$). The gate was formed by deposition of Ni/Au into an opening on the 100 nm thick SiN dielectric to allow for edge termination. A device image is presented in Fig. 1.

DC characterization was carried out using an Agilent 4156C parameter analyzer using Be/Cu probe tips. A Tektronix 370A Curve Tracer was used to collect high voltage I-V curves, with a maximum power setting of 2 W to protect the device. An Agilent B114A pulse generator and an Agilent DSO7054B oscilloscope were used to collect pulsed data. A Wentworth automated temperature control chuck was used to vary the chuck temperature from room temperature to 500°C. At each temperature tested, a minimum of 5 minutes was allowed for the sample to reach uniform steady-state temperature before measurement was carried out. Due to convection, radiation, and imperfect contact of the wafer to the heating chuck, the deviations between the chuck and device temperature were 0, 2 and 5°C at the chuck temperatures of 200, 400 and 500°C, respectively, as confirmed by a contactless IR temperature probe. Then the device temperatures were adjusted to the set temperatures.

III. RESULTS AND DISCUSSION

In Fig. 2, typical current-voltage characteristics are shown at select temperatures from room temperature to 500°C. A unique characteristic of these n-channel HEMTs is the ability of the gate to enhance current flow ($V_g = +10$ V) at moderately high V_{DS} (> 10 V) before gate leakage current becomes significant (>100 nA). The knee voltages did not exhibit significant change during testing, indicating that the devices performance is primarily limited by Ohmic contact resistance [26]. This result is also confirmed by observation of the low-field region, as the drain I-V curves appears almost Schottky-like but upon heating becomes Ohmic as thermal energy becomes sufficient to lower the energy barrier of the quasi-Ohmic contacts.

TABLE 1. Comparison of common semiconductors and wide bandgap semiconductors material properties and figure of merits relative to Si.

Properties	Si	GaAs	4H-SiC	GaN	Ga_2O_3	$Al_{0.7}Ga_{0.3}N$	AlN
Bandgap, E_g (eV)	1.12	1.42	3.25	3.4	4.85	5.7	6.2
Dielectric constant, ε	11.8	12.9	9.7	9	10	8.86	8.5
Breakdown Field, E_c (MV/cm)	0.3	0.4	2.5	3.9	8	12.7	12
Electron Mobility, μ ($cm^2/V{\cdot}s$)	1500	8500	1000	1250	300	310	1090
Maximum Velocity, V_s (10^7 cm/s)	1	1	2	3	2	1.6	2.2
Thermal Conductivity, λ (W/cm·K)	1.5	0.5	4.9[11]	2.53[15]	0.23[16]	0.07[17]	2.85[18]
Figure of Merit Relative to Si							
Johnson – $E_c^2{\cdot}V_s^2/4\pi^2$	1	1.78	278	1089	2844	4588	7744
Baliga – $\varepsilon \cdot \mu \cdot E_c^3$	1	14.7	317	846	3214	11773	335006
Baliga High Frequency – $\mu \cdot E_c^2$	1	10.1	46.3	101	142	370	1163
Keyes – $\lambda \cdot [(c{\cdot}V_s)/(4\pi{\cdot}\varepsilon)]^{1/2}$	1	0.32	3.6	1.8	0.2	0.7	1.07

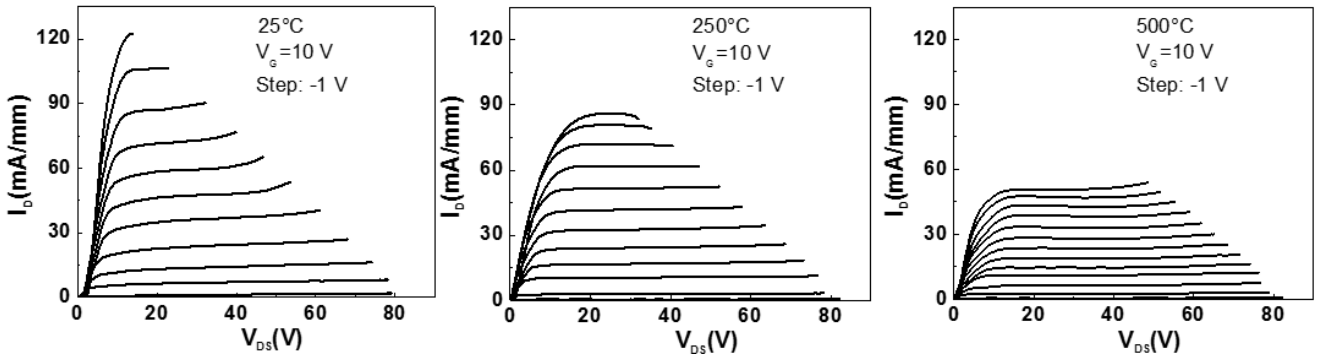

FIGURE 2. I_{DS}-V_{DS} curves for AlGaN-channel devices from 25-500°C.

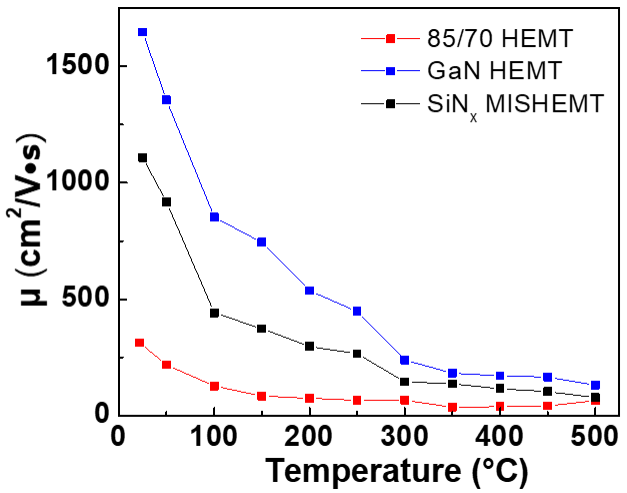

FIGURE 3. Electron mobility as a function of temperature for 85/70 HEMT, GaN HEMT($Al_{0.25}Ga_{0.75}N$/GaN) and SiN_x–gate insulator MISHEMT ($Al_{0.26}Ga_{0.74}N$/GaN).

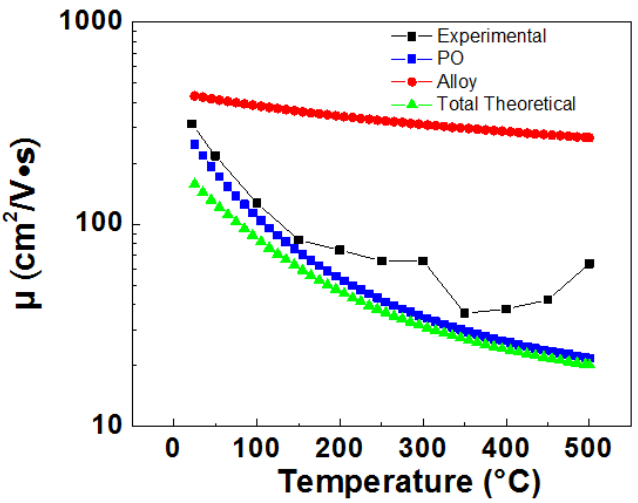

FIGURE 4. Calculated and experimental mobility of 2D electron gas in AlGaN channel as a function of temperature with contributions of alloy scattering and polar optical phonon scattering considered.

Approximately 58% reduction of total current flow from room temperature to 500°C was observed and can primarily be attributed to a lower electron mobility. Fig. 3 presents a comparison of the experimentally observed electron mobility in the novel 85/70 structure along with a traditional GaN HEMT($Al_{0.25}Ga_{0.75}N$/GaN) and a SiN_x–gate insulator MISHEMT ($Al_{0.26}Ga_{0.74}N$/GaN). Both traditional GaN HEMT, MISHEMT, and 85/70 HEMT utilized a Ni/Au Schottky gate. The mobility was extracted from the

low-electric-field (V_{gs} = 2, 4, 6 V and V_{ds} = 0 to 2 V) current-voltage characteristics through use of the following equation:

$$\frac{V_{DS}}{I_{DS}} = R_S + R_D + \frac{Ld}{\mu W \varepsilon (V_{GS} - V_{OFF})}$$

where V_{DS} and I_{DS} are the drain to source voltage and current, respectively. R_S and R_D are the source and drain resistances, L is the gate length, W is the channel width, d is the thickness of the barrier layer, ε is the dielectric constant, V_{GS} is the applied gate voltage, and V_{OFF} is the pinchoff voltage. To ensure accurate extraction of the low field mobility the result was compared to that of contactless C-V measurement. The mobility of the 85/70 device is expected to be lower than that of both GaN devices due to a larger effective electron mass. The predominant factors limiting the performance of the alloyed channel HEMT device are alloy scattering (A) and polar optical phonon scattering (PO). Thus, the discussion of the mobility will be limited to these two factors. For our purposes, the total mobility can be calculated as an inverse summation of the individual contributing mechanisms as described by Matthiessen's Rule:

$$\frac{1}{\mu} = \sum \frac{1}{\mu_i} = \frac{1}{\mu_A} + \frac{1}{\mu_{PO}} + \cdots$$

The Harrison-Hauser expression was used to the describe the temperature dependence of alloy scattering [28]:

$$\mu_A = \frac{32q(\hbar)^4}{9\sqrt{2}\pi^{\frac{3}{2}}\Omega_0 x(1-x)(\Delta E)^2 (m^*)^{\frac{5}{2}} (kT)^{1/2}}$$

where q is the charge of an electron, h is Planck's constant, m* is the effective electron mass, ΔE is the scattering potential taken as the difference in conduction band electron energies of the two binary alloys (e.g., AlN and GaN), and Ω_0 is the unit cell volume. ΔE is most commonly calculated by taking the difference in the electron affinities of the two materials. The Harrison-Hauser equation shows a direct $T^{-1/2}$ relation of mobility to temperature; however, the electron mass is assumed to be constant which is not fully correct and is a limitation of the model. A result found by Hoffman *et al.* describes the effective electron mass in GaN channel HEMT structures to be strongly related to temperature [29]. Below 100 K, m* is approximately constant, and from 100K to 300K, m* nearly doubles. There was no report on the GaN m* above 300K. The effective electron mass increases with temperature due primarily to the reduction in the confinement of the 2DEG, which leads to the increased hybridization of the envelope wave function of the heterostructure conduction band edge [29], [30]. Stradling and Wood found a similar case for narrow bandgap materials (InSb, InAs, and GaAs), and observed that the effective electron mass reaches a maximum value and then will begins to decrease with temperature [31]. For these narrow bandgap materials, the maximum effective electron mass value is reached at

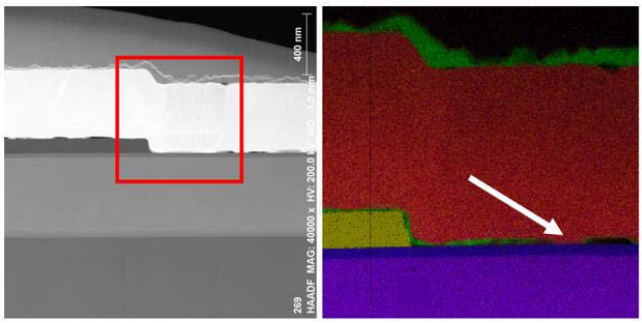

(a) (b)

FIGURE 5. **(a) STEM image of device gate area and (b) elemental analysis of gate area. Red is Au, green is Ni-O, yellow is SiN, and purple is AlGaN.**

fairly low temperatures (< 100 K) [31], [32]. It is quite possible that if Hoffman *et al.* had continued to measure effective electron mass at high temperatures, a maximum value of effective electron mass would have been reached, albeit at a high temperature in excess of 300 K.

To model PO scattering a result by Petritz and Scanlon was used and is given by:

$$\mu_{PO} = \frac{8(\hbar)^2}{3qm_0(2\pi m_0 k\theta)^{0.5}} \left(\frac{1}{\varepsilon_\infty} - \frac{1}{\varepsilon_s}\right)^{-1} \left(\frac{m_0}{m^*}\right)^{\frac{1}{2}} \times \frac{\chi\left(\frac{\Theta}{T}\right)(e^{\frac{\Theta}{T}} - 1)}{\left(\frac{\Theta}{T}\right)^{1/2}}$$

where Θ is the longitudinal optical phonon temperature, m_0 is the free effective electron mass, ε_8 is the high frequency relative dielectric constant, and ε_s is the static relative dielectric constant. $\chi(\Theta/T)$ is a temperature dependent factor that arises from use of the variational method to solve the Boltzmann equation for electronic conduction in a crystal in which scattering is due to polarization waves of the lattice and is defined by Howarth and Sondheimer [33]. Of note, both models do not account for 2DEG sheet density; this is acceptable for this study due to the wide bandgap of the channel material. The two-dimensional electron gas density in the GaN HEMT structures was found to primarily increase due to electron contributions from the bulk GaN of the HEMT structure [35]. Due to the higher bandgap of the AlGaN channel, electron contributions are expected to be much lower for the bulk material at elevated temperatures, thus the 2DEG density is basically constant.

By comparing these two mechanisms over the tested temperature range, it is observed that PO scattering is the dominant limiting mechanism at elevated temperature and is much more temperature dependent than alloy scattering, Fig. 4. At moderate temperatures, less than 250 K, alloy scattering will become dominant and this confirms the previous work by Coltrin *et al.* [5], [6]. The experimental mobility fits fairly well to the modelled mobility but begins to deviate at very high temperatures. This deviation and kink in the experimental data at 350°C is most likely due to gate metal reordering and nickel oxidation.

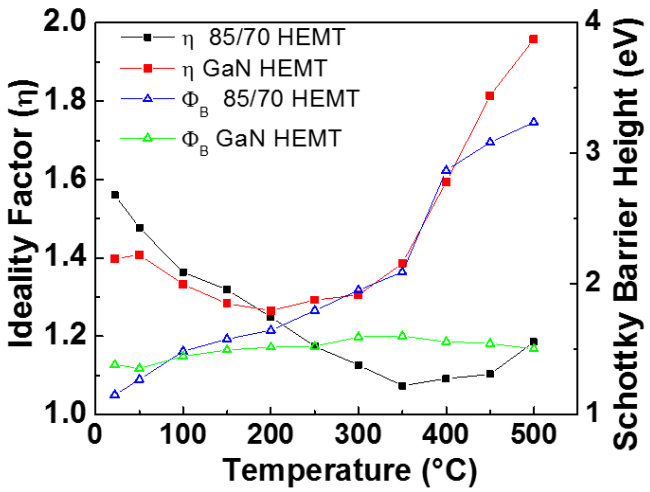

FIGURE 6. Comparison of the Ideality Factor and zero bias Schottky Barrier Height of 85/70 HEMT and traditional GaN HEMT($Al_{0.25}Ga_{0.75}N$/GaN).

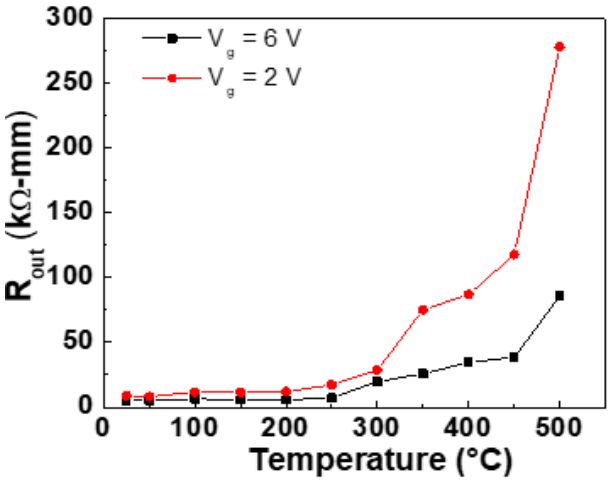

FIGURE 8. Output resistance taken at 1 W load line of I-V curves at $V_g = +2V$ and $V_g = +6$ V from 25-500°C.

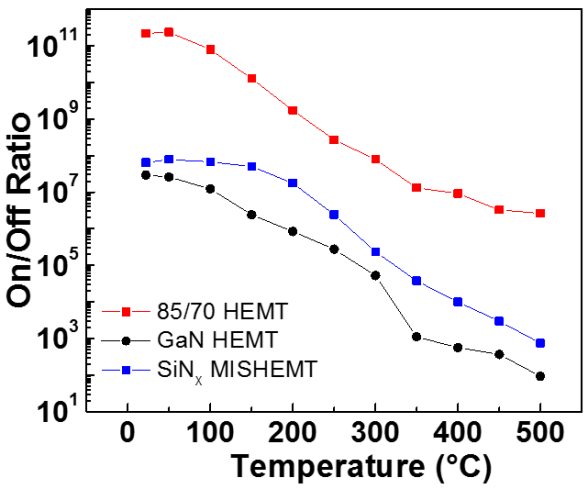

FIGURE 7. I_{ON}/I_{OFF} ratio for 85/70 HEMT compared to metal-gate GaN HEMT($Al_{0.25}Ga_{0.75}N$/GaN) and SiN_X–gate insulator MISHEMT ($Al_{0.26}Ga_{0.74}N$/GaN).

To confirm this suspicion of gate metal reordering and nickel oxidation, TEM was performed, with results shown in Fig. 5. The devices gate area is imaged in Fig. 5a and the area for elemental analysis outlined in a box. In Fig. 5b, elemental analysis confirms that gate metal reordering occurred, as the Au (marked with an arrow) is now in contact with the AlGaN barrier layer. It does not appear that the Au has penetrated and diffused into the barrier layer. Ni/Au is known to form island-like crystalline Ni-O and form a network of Au grains which will begin to diffuse to the barrier layer [36]. This potential reliability problem for high-temperature operation can be easily mitigated through use of refractory metals for the gate contact and by optimizing the gate metal thicknesses, which is the subject of future work.

As the gate provides modulation across the full temperature range, its characteristics were extracted next. In Fig. 6, the zero bias SBH and Ideality Factor are plotted versus temperature. The SBH was extracted through use of the thermionic emission model:

$$I = I_0 \exp\left(\frac{qV}{nkT}\right)\left[1 - \exp\left(-\frac{qV}{kt}\right)\right]$$

$$I_0 = AA^{**}T^2 \exp\left(-\frac{q\phi_b}{kT}\right)$$

where I_0 is the reverse saturation current, V is the applied voltage, n is the ideality factor, A is effective diode area, A** is the Richardson constant, and ϕ_b is the SBH. The SBH of the 85/70 device increase significantly from room temperature to 500°C. For the traditional GaN device, the SBH changes were much less due to surface potential pinning by the surface counter charges. With lower SBHs of traditional GaN device at elevated temperature, the gate leakage current is a limiting factor for performance for traditional devices. The shifts in the ideality factor and SBH at 350°C are due to reordering of the gate metal as the elevated measurement temperature acts as a low-temperature anneal. It was observed that once the device had been heated to 350°C or higher, the gates electrical characteristics underwent a permanent change and could not be recovered which was consistent with the STEM analysis in Fig. 5. Lower test temperatures always gave full recovery to initial state.

In Fig. 7, the I_{ON}/I_{OFF} ratio of the devices are shown as a function of temperature and demonstrate the much-improved performance of the 85/70 HEMT over the traditional GaN channel devices. The lower limit of the measurement system was reached for the 85/70 devices at room temperature and 50°C at a current level of 1 fA, and the ratio is likely larger than what is reported. For the 85/70 device, the ratio decreases with temperature primarily because of leakage current. For the traditional devices, the leakage current became very large at high temperature, along with greater reduction in I_{ON}. Only limited works have explored the extreme temperature operation of GaN

HEMTs above 200-300°C as the devices lose the ability to be fully pinched off and are not suited for such applications [37], [38]. The high I_{ON}/I_{OFF} ratio is quite promising for high temperature applications and can potentially bring great savings in cooling requirements for devices used for such purposes. The similar slope for all the devices can be attributed to the leakage current stemming from the same mechanism, Frenkel-Poole emission.

To further emphasize the capability of the 85/70 HEMT, the output resistance of the device was calculated at gate voltages of 2 V and 6 V (along the 1 W load line of drain I-Vs), with the result shown in Fig. 8. Ideal MOSFET performance is achieved when the drain current is not influenced by drain to source voltage while operating in the saturation regime, i.e., infinite output resistance. A finite output resistance lowers the gain of the device and limits performance. For the 85/70 HEMT this ideal behavior is closer to being realized than for traditional HEMT, especially at high temperatures with resistances in the 100's of kΩ. This further shows the superior performance of the AlGaN-channel HEMT at high temperatures.

To investigate the leakage current of the 85/70 devices, the activation energy of the gate-induced drain leakage current was extracted, as shown in Fig. 9a and Fig. 9b. Of note is that in Fig. 9a, the deep subthreshold voltage is relatively invariant across the measured temperature range. This result indicates that the 2DEG channel does not open or close slower regardless of heating, which is advantageous for simplifying circuit design as the same threshold voltage may be assumed regardless of operating temperature. An Arrhenius form was assumed to extract the activation energy. Two regimes were found, from 100°C to 350°C and 350°C to 500°C with activation energies $E_a = 0.63$ eV and $E_a = 0.076$ eV, respectively. For the 100 to 350°C range the leakage mechanism is consistent with trap-assisted Poole Frenkel emission, as previously reported for these structures by Baca *et al.* [9]. For traditional GaN channel devices, Poole Frenkel current is the primary mechanism for leakage current, provided that bulk current is negligible [37]–[41]. For the high temperature regime, as the activation energy is very near zero ($E_a = 0.076$ eV), a secondary mechanism is now dominant. This is likely band-to-band tunneling [42], [43]. Band-to-band tunneling does not rely on mid-gap traps, but rather depends upon the bending of the conduction and valence band being large enough such that direct tunneling becomes possible. Deep-level transient spectroscopy or other similar defect spectroscopy techniques would be of use to further investigate the trapping mechanisms and to obtain precise measurement of trap energy levels. Previous work on AlGaN/GaN HEMT devices has explained this low trap activation energy by direct tunneling of electrons into near band edge defect states, followed by Pool-Frenkel activation of those captured electrons [41].

To further verify the presence of interfacial traps, gate-lag measurements were performed at 100 kHz and 10% duty cycle (1 μs pulses), as shown in Fig. 10. Near ideal

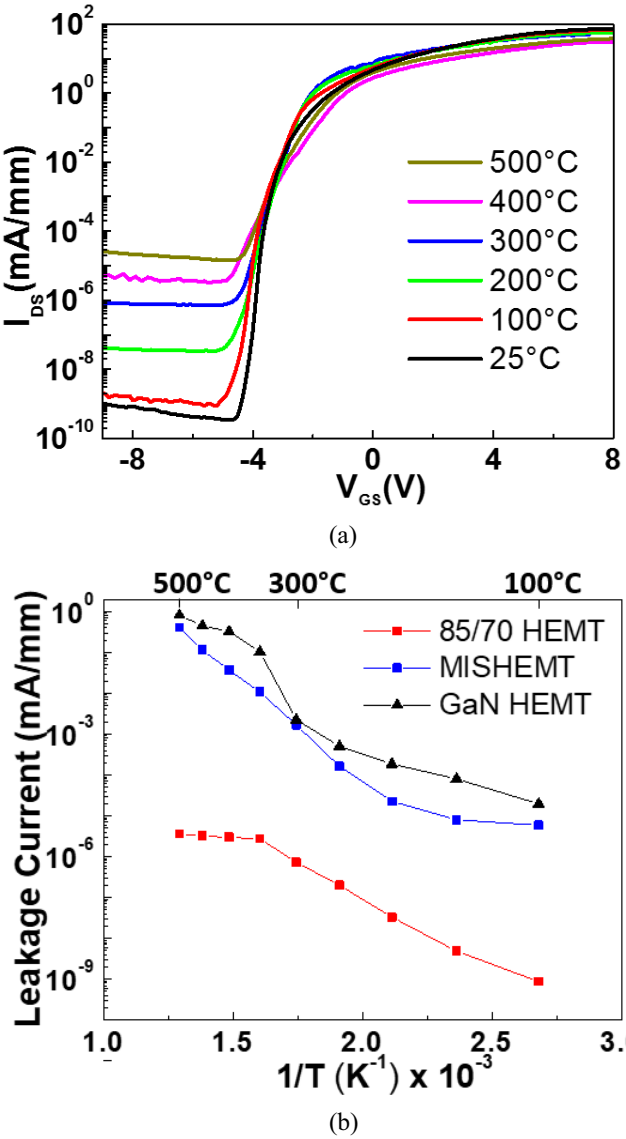

FIGURE 9. (a) I_{DS}-V_G plot at V_{DS} = 10 V at select temperatures and (b) Arrhenius plot of gate induced drain leakage current.

characteristics were observed at all temperatures, with only slight lowering at high gate voltages upon heating. The ideal matching of DC to pulsed current indicates that a high-quality interface has been formed during growth of the HEMT structure, with minimal surface states. The subthreshold swing values were used to quantify the heterointerfacial traps present, as shown in Fig. 11, using the relation:

$$S = \frac{kT}{q}\ln(10)\left(1 + \frac{D_{it}q}{C_{AlGaN}}\right)$$

where S is the subthreshold swing, C_{AlGaN} is the capacitance of the AlGaN layer, and D_{it} is the interfacial trap density. First, at room temperature a low subthreshold swing value of 80 mV/dec was observed, which is near the ideal value of 63 mV/dec. Across the temperature range, there are two distinct regions, namely 25 to 300°C and 300 to

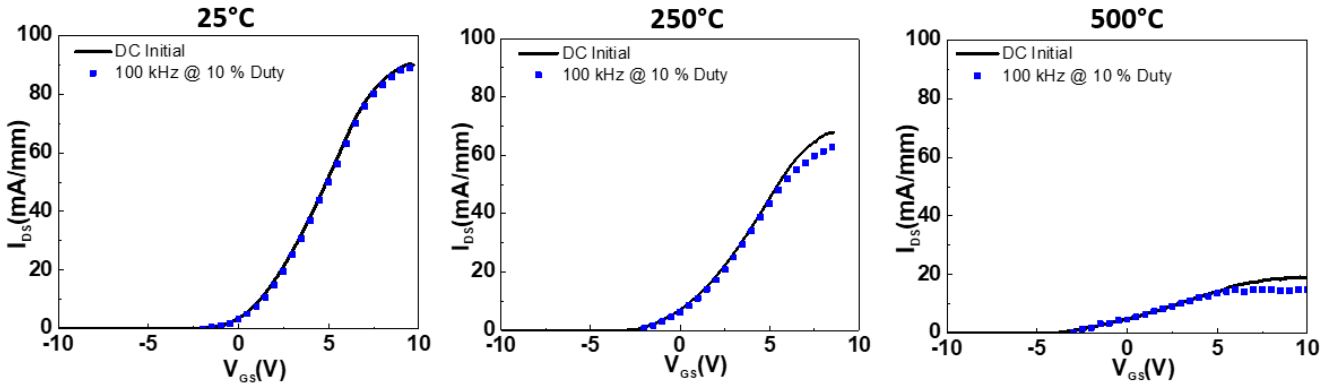

FIGURE 10. Gate-lag measurement at select temperatures (V_{DS} = 10 V).

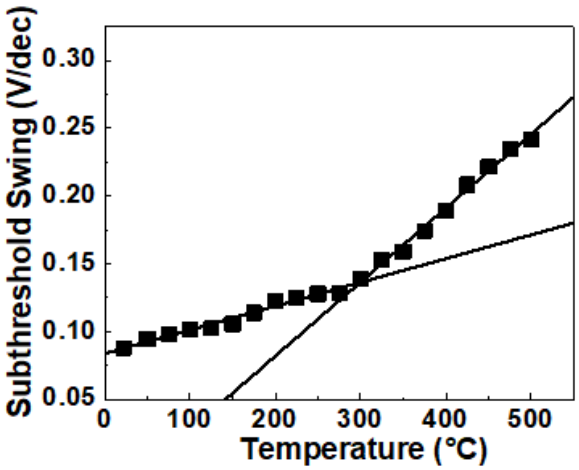

FIGURE 11. Subthreshold swing as a function of temperature has two distinct linear regimes.

350°C with extracted trap densities of 2×10^{11} cm^{-2} and 3×10^{12} cm^{-2}, respectively. The increased trap density can also be attributed to thermal activation of mid-gap traps beginning at 300°C. To investigate if gate metal reordering introducing additional the trap density, the sample was cooled back down to room temperature to see if the drain and gate IVs recovered. There were no changes for IVs observed until 350°C indicating that the gate metal reordering did not occur until 350°C. If gate metal reordering was predominant rather than heterointerfacial, it would be expected a third regime at 350°C in Fig. 11. As the third regime is not present, this effect is likely negligible.

IV. CONCLUSION

The novel $Al_{0.85}Ga_{0.15}N/Al_{0.7}Ga_{0.3}N$ HEMT structures demonstrate much improved performance over traditional GaN-channel HEMT devices for extreme temperature operation. With only 58% reduction of DC current at 500°C compared to room temperature, and minimal loss in switching current as observed by gate-lag, there is great potential for these high power switching AlGaN HEMTs. The exceedingly low leakage current is also very favorable for potential power savings. The primary limiting factor at the present is the Ohmic contacts, which can be improved through the use of graded heterostructures and further metallization optimization. This technology in its present state is quite promising, as it requires little change from current GaN processing techniques and may be simpler to implement than entirely new wide bandgap semiconductors that have not yet been brought to market. Use of refractory metals may aid in the further development of this new HEMT structure for extreme temperature applications.

ACKNOWLEDGMENT

This paper describes objective technical results and analysis. Any subjective views or opinions that might be expressed in the paper do not necessarily represent the views of the U.S. Department of Energy or the United States Government.

REFERENCES

[1] T. Nanjo *et al.*, "AlGaN channel HEMT with extremely high breakdown voltage," *IEEE Trans. Electron Devices*, vol. 60, no. 3, pp. 1046–1053, Mar. 2013. doi: 10.1109/TED.2012.2233742.

[2] M. Hatano *et al.*, "Comparative high-temperature DC characterization of HEMTS with GaN and AlGaN channel layers," in *Proc. CS MANTECH Conf.*, Portland, OR, USA, May 2010 p. 101.

[3] A. Baca *et al.*, "High temperature operation of $Al_{0.45}Ga_{0.55}N/Al_{0.30}Ga_{0.70}N$ high electron mobility transistors," *ECS J. Solid State Sci. Technol.*, vol. 6, no. 11, pp. S3010–S3013, 2017. doi: 10.1149/2.0041711jss.

[4] N. Yafune *et al.*, "AlN/AlGaN HEMTs on AlN substrate for stable high-temperature operation," *Electron. Lett.*, vol. 50, no. 3, pp. 211–212, Jan. 2014. doi: 10.1049/el.2013.2846.

[5] M. E. Coltrin and R. J. Kaplar, "Transport and breakdown analysis for improved figure-of-merit for AlGaN power devices," *J. Appl. Phys.*, vol. 121, no. 5, 2017, Art. no. 055706. doi: 10.1063/1.4975346.

[6] M. E. Coltrin, A. G. Baca, and R. J. Kaplar, "Analysis of 2D Transport and performance characteristics for lateral power devices based on AlGaN alloys," *ECS J. Solid State Sci. Technol.*, vol. 6, no. 11, pp. S3114–S3118, 2017. doi: 10.1149/2.0241711jss.

[7] T. Nanjo *et al.*, "First operation of AlGaN channel high electron mobility transistors," *Appl. Phys. Exp.*, vol. 1, no. 1, 2007, Art. no. 011101. doi: 10.1143/APEX.1.011101.

[8] A. Baca *et al.*, "An $AlN/Al_{0.85}Ga_{0.15}N$ high electron mobility transistor," *Appl. Phys. Lett.*, vol. 109, no. 3, 2016, Art. no. 033509. doi: 10.1063/1.4959179.

[9] A. Baca *et al.*, "$Al_{0.85}Ga_{0.15}N/Al_{0.70}Ga_{0.30}N$ high electron mobility transistors with Schottky gates and large on/off current ratio over temperature," *ECS J. Solid State Sci. Technol.*, vol. 6, no. 12, pp. Q161–Q165, 2017. doi: 10.1149/2.0231712jss.

[10] R. Kaplar *et al.*, "Review—Ultra-wide-bandgap AlGaN power electronic devices," *ECS J. Solid State Sci. Technol.*, vol. 6, no. 2, pp. Q3061–Q3066, 2016. doi: 10.1149/2.0111702jss.

[11] S. Bajaj *et al.*, "Ultra-wide bandgap AlGaN channel MISFET with polarization engineered Ohmics," in *Proc. 74th Annu. Device Res. Conf. (DRC)*, Newark, DE, USA, 2016, pp. 1–2.

[12] S. Muhtadi *et al.*, "High electron mobility transistors with $Al_{0.65}Ga_{0.35}N$ channel layers on thick AlN/Sapphire templates," *IEEE Electron Device Lett.*, vol. 38, no. 7, pp. 914–917, Jul. 2017. doi: 10.1109/LED.2017.2701651.

[13] H. Tokuda *et al.*, "High Al composition AlGaN-channel high-electron-mobility transistor on AlN substrate," *Appl. Phys. Exp.*, vol. 3, no. 12, 2010, Art. no. 121003. doi: 10.1143/APEX.3.121003.

[14] H. Yu *et al.*, "Ion implanted AlGaN-GaN HEMTs with nonalloyed Ohmic contacts," *IEEE Electron Device Lett.*, vol. 26, no. 5, pp. 283–285, May 2005. doi: 10.1109/LED.2005.846583.

[15] S. Bajaj *et al.*, "Graded AlGaN channel transistors for improved current and power gain linearity," *IEEE Trans. Electron Devices*, vol. 64, no. 8, pp. 3114–3119, Aug. 2017. doi: 10.1109/TED.2017.2713784.

[16] M. Suita, T. Nanjo, T. Oishi, Y. Abe, and Y. Tokuda, "Ion implantation doping for AlGaN/GaN HEMTs," *Physica Status Solidi (c)*, vol. 3, no. 6, pp. 2364–2367, 2006. doi: 10.1002/pssc.200565135.

[17] M. Suita, T. Nanjo, T. Oishi, Y. Abe, and Y. Tokuda, "Application of lightly doped drain structure to AlGaN/GaN HEMTs by ion implantation technique," *Electron. Lett.*, vol. 44, no. 23, pp. 1378–1379, Nov. 2008. doi: 10.1049/el:20081746.

[18] T. Zimmermann, D. Deen, Y. Cao, D. Jena, and H. G. Xing, "Formation of ohmic contacts to ultra-thin channel AlN/GaN HEMTs," *Physica Status Solidi (c)*, vol. 5, no. 6, pp. 2030–2032, 2008. doi: 10.1002/pssc.200778724.

[19] E. A. Douglas, C. A. Sanchez, R. J. Kaplar, A. A. Allerman, and A. G. Baca, "Inductively coupled BCl_3/Cl_2/Ar plasma etching of Al-rich AlGaN," *J. Vac. Sci. Technol. A*, vol. 35, no. 2, 2017, Art. no. 021305. doi: 10.1116/1.4971245.

[20] D. Long and J. Myers, "Ionized-impurity scattering mobility of electrons in silicon," *Phys. Rev.*, vol. 115, no. 5, pp. 1107–1118, 1959. doi: 10.1103/PhysRev.115.1107.

[21] D. Chattopadhyay, "Electron mobility limited by ionized impurity scattering with nonlinear screening in semiconductors," *Phys. Rev. B, Condens. Matter*, vol. 23, no. 4, pp. 1847–1850, 1981. doi: 10.1103/PhysRevB.23.1847.

[22] C. H. Oxley, M. J. Uren, A. Coates, and D. G. Hayes, "On the temperature and carrier density dependence of electron saturation velocity in an AlGaN/GaN HEMT," *IEEE Trans. Electron Devices*, vol. 53, no. 3, pp. 565–567, Mar. 2006. doi: 10.1109/TED.2005.863540.

[23] R. Yahyazadeh, Z. Hashempour, and O. Marofi, "Effect of high temperature on the transconductance of AlGaN/GaN high electron mobility transistors (HEMT)," *Int. J. Acad. Res.*, vol. 5, no. 4, pp. 78–86, 2013. doi: 10.7813/2075-4124.2013/5-4/a.9.

[24] D. Maier *et al.*, "InAlN/GaN HEMTs for operation in the 1000°C regime: A first experiment," *IEEE Electron Device Lett.*, vol. 33, no. 7, pp. 985–987, Jul. 2012. doi: 10.1109/LED.2012.2196972.

[25] B. Godejohann *et al.*, "AlN/GaN HEMTs grown by MBE and MOCVD: Impact of Al distribution," *Physica Status Solidi (b)*, vol. 254, no. 8, 2017, Art. no. 1600715. doi: 10.1002/pssb.201600715.

[26] G. Li *et al.*, "Threshold voltage control in $Al_{0.72}Ga_{0.28}N$/AlN/GaN HEMTs by work-function engineering," *IEEE Electron Device Lett.*, vol. 31, no. 9, pp. 954–956, Sep. 2010.

[27] H. Okumura *et al.*, "AlN metal–semiconductor field-effect transistors using Si-ion implantation," *Jpn. J. Appl. Phys.*, vol. 57, no. 4, 2018, Art. no. 04FR11. doi: 10.7567/JJAP.57.04FR11.

[28] J. W. Harrison and J. R. Hauser, "Alloy scattering in ternary III-V compounds," *Phys. Rev. B, Condens. Matter*, vol. 13, no. 12, pp. 5347–5350, 1976. doi: 10.1103/PhysRevB.13.5347.

[29] T. Hofmann *et al.*, "Temperature dependent effective mass in AlGaN/GaN high electron mobility transistor structures," *Appl. Phys. Lett.*, vol. 101, no. 19, 2012, Art. no. 192102. doi: 10.1063/1.4765351.

[30] A. Kurakin *et al.*, "Quantum confinement effect on the effective mass in two-dimensional electron gas of AlGaN/GaN heterostructures," *J. Appl. Phys.*, vol. 105, no. 7, 2009, Art. no. 073703. doi: 10.1063/1.3100206.

[31] R. Stradling and R. Wood, "The temperature dependence of the band-edge effective masses of InSb, InAs and GaAs as deduced from magnetophonon magnetoresistance measurements," *J. Phys. C Solid State Phys.*, vol. 3, no. 5, pp. L94–L99, 1970. doi: 10.1088/0022-3719/3/5/005.

[32] N. Cavassilas, J.-L. Autran, F. Aniel, and G. Fishman, "Energy and temperature dependence of electron effective masses in silicon," *J. Appl. Phys.*, vol. 92, no. 3, pp. 1431–1433, 2002. doi: 10.1063/1.1490620.

[33] D. J. Howarth and E. H. Sondheimer, "The theory of electronic conduction in polar semi-conductors," *Proc. Roy. Soc. London A Math. Phys. Eng. Sci.*, vol. 219, no. 1136, pp. 53–74, 1953. doi: 10.1098/rspa.1953.0130.

[34] M. Wang *et al.*, "High temperature dependence of the density of two-dimensional electron gas in $Al_{0.18}Ga_{0.82}N$/GaN heterostructures," *Appl. Phys. A, Solids Surf.*, vol. 88, no. 4, pp. 715–718, 2007. doi: 10.1007/s00339-007-4034-5.

[35] M. T. Hasan, H. Tokuda, and M. Kuzuhara, "Surface barrier height lowering at above 540 K in AlInN/AlN/GaN heterostructures," *Appl. Phys. Lett.*, vol. 99, no. 13, 2011, Art. no. 132102. doi: 10.1063/1.3644161.

[36] L.-C. Chen *et al.*, "Oxidized Ni/Pt and Ni/Au ohmic contacts to p-type GaN," *Appl. Phys. Lett.*, vol. 76, no. 25, pp. 3703–3705, 2000.

[37] W. S. Tan *et al.*, "High temperature performance of AlGaN/GaN HEMTs on Si substrates," *Solid-State Electron.*, vol. 50, no. 3, pp. 511–513, 2006. doi: 10.1016/j.sse.2006.02.008.

[38] A. Fontserè *et al.*, "Molecular beam epitaxial AlGaN/GaN high electron mobility transistors leakage thermal activation on silicon and sapphire," *Appl. Phys. Lett.*, vol. 102, no. 9, 2013, Art. no. 093503. doi: 10.1063/1.4794411.

[39] S. Turuvekere *et al.*, "Gate leakage mechanisms in AlGaN/GaN and AlInN/GaN HEMTs: Comparison and modeling," *IEEE Trans. Electron Devices*, vol. 60, no. 10, pp. 3157–3165, 2013. doi: 10.1109/TED.2013.2272700.

[40] Y. Chen *et al.*, "Study of surface leakage current of AlGaN/GaN high electron mobility transistors," *Appl. Phys. Lett.*, vol. 104, no. 15, 2014, Art. no. 153509. doi: 10.1063/1.4871736.

[41] S. Ganguly, A. Konar, Z. Hu, H. Xing, and D. Jena, "Polarization effects on gate leakage in InAlN/AlN/GaN high-electron-mobility transistors," *Appl. Phys. Lett.*, vol. 101, no. 25, 2012, Art. no. 253519. doi: 10.1063/1.4773244.

[42] A. Alnuaimi, A. Nayfeh, and V. Koldyaev, "Electric-field and temperature dependence of the activation energy associated with gate induced drain leakage," *J. Appl. Phys.*, vol. 113, no. 4, 2013, Art. no. 044513. doi: 10.1063/1.4789382.

[43] S. Geissler, E. Adler, and R. Bolam, "A thermally activated gate current in off-state PMOSFETs," in *Proc. 29th Annu. Rel. Phys.*, Las Vegas, NV, USA, 1991, pp. 123–128.

[44] X. Qian, P. Jiang, and R. Yang, "Anisotropic thermal conductivity of 4H and 6H silicon carbide measured using time-domain thermoreflectance," *Mater. Today Phys.*, vol. 3, pp. 70–75, Dec. 2017. doi: 10.1016/j.mtphys.2017.12.005.

[45] H. Shibata *et al.*, "High thermal conductivity of gallium nitride (GaN) crystals grown by HVPE process," *Mater. Trans.*, vol. 48, no. 10, pp. 2782–2786, 2007. doi: 10.2320/matertrans.mrp2007109.

[46] Z. Galazka *et al.*, "On the bulk β-Ga2O3 single crystals grown by the Czochralski method," *J. Cryst. Growth*, vol. 404, pp. 184–191, Oct. 2014. doi: 10.1016/j.jcrysgro.2014.07.021.

[47] W. Liu and A. Balandin, "Thermal conduction in AlxGa1-xN alloys and thin films," *J. Appl. Phys.*, vol. 97, no. 7, 2005, Art. no. 073710. doi: 10.1063/1.1868876.

[48] G. A. Slack, R. A. Tanzilli, R. O. Pohl, and J. W. Vandersande, "The intrinsic thermal conductivity of AlN," *J. Phys. Chem. Solids*, vol. 48, no. 7, pp. 641–647, 1987. doi: 10.1016/0022-3697(87)90153-3.

PATRICK H. CAREY, IV is currently pursuing the graduation degree with the Department of Chemical Engineering, University of Florida, Gainesville, FL, USA. His research interests include fabrication and characterization of compound semiconductors, along with fabrication of antibacterial coatings for dental implants.

FAN REN (F'10) was with AT&T Bell Laboratories for 12 years. He joined the University of Florida, Gainesville, FL, USA, in 1997, where he is a Distinguished Professor. He is a fellow of the Electrochemical Society, Materials Research Society, Society of Photographic Instrumentation Engineers, American Physical Society, and American Vacuum Society.

ALBERT G. BACA received the Ph.D. degree in chemistry from the University of California, Berkeley, in 1985. He was with AT&T Bell Laboratories for five years. In 1990, he joined Sandia National Laboratories, where he is a Distinguished Member of the Technical Staff. His research interests are in III-V semiconductor device and device reliability. He is a fellow of Electrochemical Society.

BRIANNA A. KLEIN received the B.S. and M.S. degrees from the New Mexico Institute of Mining and Technology in 2008 and 2009, respectively, and the Ph.D. degree from the University of New Mexico in 2014. Her research interests are in III-N transistors and III-V semiconductor optoelectronics.

ANDREW A. ALLERMAN received the Ph.D. degree in physics from Auburn University, Auburn, AL, USA, in 1992. He is currently a Principal Member of Technical Staff with Sandia National Laboratories, Albuquerque.

ANDREW M. ARMSTRONG received the Ph.D. degree in electrical and computer engineering from Ohio State University in 2006. He is a Principle Member of the Technical Staff with the Semiconductor Material and Devices Sciences Department, Sandia National Laboratories.

ERICA A. DOUGLAS received the Ph.D. degree in materials science and engineering from the University of Florida in 2011. In 2012, she joined Sandia National Laboratories. She currently serves on the Electronic Materials and Photonics Division Executive Committee for the American Vacuum Society, as well as the Electronics and Photonics Division Executive Committee for the Electrochemical Society.

ROBERT J. KAPLAR (M'04–SM'17) received the B.S. degree in physics from Case Western Reserve University, Cleveland, OH, USA, and the M.S. and Ph.D. degrees in electrical engineering from Ohio State University, Columbus, OH, USA. He is a currently the Manager of the Semiconductor Material and Device Sciences Department, Sandia National Laboratories, Albuquerque, NM, USA.

PAUL G. KOTULA is a Staff Member with the Materials Characterization Department, Sandia National Laboratories, Albuquerque, NM, USA. He has helped build a research program on spectral imaging and multivariate statistical analysis. He is currently the President-Elect of the Microscopy Society of America.

STEPHEN J. PEARTON received the Ph.D. degree in physics from the University of Tasmania. He was AT&T Bell Laboratories from 1994 to 2004. He is a Distinguished Professor with the University of Florida, Gainesville, FL, USA. He was a recipient of the 2007 J. J. Ebers Award from IEEE.